



Complete oxidation of formaldehyde at room temperature over Ag-loaded octahedral molecular sieve synthesized from solvent-free route

Ling Zhang^a, Shichao Han^b, Yingjuan Wu^c, Yiquan Xie^c, Liang Wang^a, Xiangju Meng^{c,*}, Feng-Shou Xiao^{a,*}

^a Key Lab of Biomass Chemical Engineering of Ministry of Education, College of Chemical and Biological Engineering, Zhejiang University, Hangzhou 310027, China

^b Zhejiang Key Laboratory of Urban Environmental Processes and Pollution Control, Ningbo Urban Environment Observation and Research Station, Chinese Academy of Sciences, Ningbo 315800, China

^c Department of Chemistry, Zhejiang University, Hangzhou 310028, China



ARTICLE INFO

Keywords:

Formaldehyde
Complete oxidation
Room temperature
Ag-based catalysts
OMS-2-S

ABSTRACT

Removal of formaldehyde (HCHO) has recently been attracted much attention, and completely catalytic oxidation at room temperature has been identified as one of the efficient routes for solving this problem. In this research, we show a successful preparation of Ag-loaded octahedral molecular sieve from solvent-free route (Ag/OMS-2-S), which was characterized by XRD, SEM, HRTEM, BET, XPS, ICP-OES, H₂-TPR, and HCHO-TPD techniques to investigate the factors influencing the catalytic activity. Very interestingly, HCHO is completely converted into CO₂ at room temperature over the Ag/OMS-2-S catalyst. To the best of our knowledge, this is the first time for complete oxidation of HCHO at room temperature over all the Ag-based catalysts. Relating to the characterizations, it is suggested that the active oxygen species play a key factor that contributes to the excellent performance of the Ag/OMS-2-S. In addition, the Ag/OMS-2-S catalyst is also very stable and selective. Combination of extraordinary activity and excellent stability of the Ag/OMS-2-S catalysts might offer an alternative way to develop new efficient catalysts for the removal of air pollutants.

1. Introduction

Formaldehyde (HCHO) is one of the major components of indoor air pollutants, which is mainly emitted from widely used building and decorative materials [1–4]. Exposure to HCHO for a long time may cause headache, respiratory tract, pneumonia, eye irritation, and even cancer. Therefore, a highly efficient abatement of HCHO is urgently needed in order to protect human health, and then a series of approaches for HCHO removal such as adsorption [5,6], photo-catalytic oxidation [7,8], plasma decomposition [9,10], and catalytic oxidation [2–4] have been developed during past decades. Among them, catalytic oxidation has been identified as one of the most effective, economically feasible, and promising routes for HCHO abatement due to its non-toxic by-products and high activity at low temperatures [11–16].

Supported metals (Pt, Pd, Au, Rh, Ag, Mn, and Co) [17–23] are the most useful catalysts for the catalytic oxidation of HCHO. Notably, costly metals such as Pt, Pd, Au, Rh are very active, even complete conversion of HCHO at room temperature, but relatively low-cost metals such as Ag, Mn, and Co have much lower activity. Therefore, it still

remains a challenge to develop low-cost metal-based catalysts.

Recently, Ag-based catalysts have been paid much attention in the catalytic oxidation of HCHO, due to their low price and high activity at relatively low temperatures [24–27]. For examples, He et al. investigated catalytic oxidation of HCHO at low temperature over Ag-based catalysts with different supports (TiO₂, Al₂O₃ and CeO₂) [24], and they found that Ag/TiO₂ was excellently active, giving complete conversion of HCHO at 95 °C; Li et al. reported that Ag/CeO₂ nanosphere catalysts prepared by a one-step hydrothermal method exhibited high catalytic activity, reaching to complete oxidation of HCHO at above 110 °C [25]; Our group showed that Mn-promoted Ag catalyst supported on pure silica Beta zeolite with a good hydrophobicity is very active for catalytic combustion of HCHO, displaying the complete conversion of HCHO at around 45 °C [28]. Currently, Ag-based catalysts are still difficult for complete oxidation of HCHO at room temperature.

It is worth noting that octahedral molecular sieve (OMS-2) is highly efficient for catalytic oxidation of air pollutants because of its peculiar tunnel structures of manganese oxides [29–32]. For examples, Hao et al. carried out catalytic oxidation of HCHO over three manganese oxides

* Corresponding authors.

E-mail addresses: mengxj@zju.edu.cn (X. Meng), fsxiao@zju.edu.cn (F.-S. Xiao).

with different square tunnel sizes (pyrolusite, cryptomelane and todorokite) [33], and they found that OMS-2 was the most active catalyst, because its micropores of $0.46 \times 0.46 \text{ nm}^2$ are suitable for adsorption of HCHO; Suib et al., Takeuchi et al., and King et al. showed OMS-2 supported Ag catalyst (Ag/OMS-2) was active for gas-phase catalytic oxidation of VOCs [34–36]. Herein, we have prepared Ag-loaded OMS-2-S from solvent-free route (Ag/OMS-2-S). Very importantly, the Ag/OMS-2-S showed complete conversion of HCHO at room temperature. In contrast, the Ag/OMS-2 obtained from hydrothermal method (Ag/OMS-2-L) exhibited complete conversion of HCHO at 35°C . This phenomenon is reasonably related to the formation of more active oxygen species in the Ag/OMS-2-S than those in the Ag/OMS-2-L.

2. Experimental

2.1. Materials

KMnO₄, HNO₃, and AgNO₃ were purchased from Sinopharm Chemical Reagent. Mn(Ac)₂·4H₂O and MnSO₄·H₂O were purchased from Aladdin. All these reagents were of analytical grade and used without further purification.

2.2. Preparation of catalysts

Synthesis of K-OMS-2-S. As a typical run, 9.489 g (0.06 mol) of KMnO₄ and 22.059 g (0.09 mol) of Mn(Ac)₂·4H₂O (KMnO₄:Mn(Ac)₂·4H₂O at 2:3) powders were mixed and ground in a mortar [37]. Then, the mixed powders were transferred into an autoclave for crystallization at 80°C for 4 h. The black sample was thoroughly washed with deionized water at room temperature and dried at 100°C in air overnight, which was designated as K-OMS-2-S.

Synthesis of K-OMS-2-L. As a typical run, 0.4 M solution of KMnO₄ (13.3 g in 225 mL of deionized water) was added to a mixture of 1.75 M solution of MnSO₄·H₂O (19.8 g in 67.5 mL deionized water) and 6.8 mL of concentrated HNO₃ [29], forming black precipitate. After stirring and refluxing at 100°C for 24 h, the black precipitate was washed with deionized water at room temperature and dried at 100°C in air overnight, which was designated as K-OMS-2-L.

Ag-loaded OMS-2 (Ag/OMS-2). The Ag-loaded OMS-2 catalysts were prepared by impregnation with AgNO₃. After impregnation, the excessive water was removed in a rotary evaporator at 80°C . The samples were dried at 120°C for 12 h and then calcined at 450°C for 4 h.

2.3. Characterizations

All of samples were characterized by X-ray diffraction (XRD), N₂ adsorption-desorption isotherms, plasma atomic emission spectrometry (ICP-AES), scanning electron microscopy (SEM), high-resolution TEM (HRTEM), hydrogen temperature-programmed reduction (H₂-TPR), X-ray photoelectron spectra (XPS), and formaldehyde adsorption-desorption (HCHO-TPD). The details are described in the [supplementary data](#).

2.4. Catalytic oxidation of HCHO

The catalytic activity of formaldehyde oxidation was tested in a fixed-bed quartz tube reactor (4 mm i.d.) with 0.1 g of catalyst (40–60 mesh). HCHO gas was generated by using a He bubbler. The detailed conditions are described in the [supplementary data](#).

3. Results and discussion

3.1. Catalyst characterizations

Fig. 1 showed XRD patterns of OMS-2-S, OMS-2-L, 10%Ag/OMS-2-S, and 10%Ag/OMS-2-L catalysts, giving the peaks assigned to OMS-2

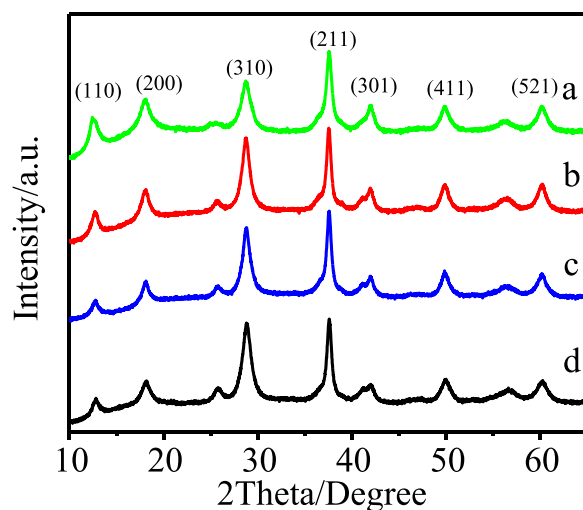


Fig. 1. XRD patterns of (a) OMS-2-S, (b) OMS-2-L, (c) 10%Ag/OMS-2-S, and (d) 10%Ag/OMS-2-L catalysts.

structure. In these samples, it was undetectable for the peaks related to Ag (2θ at 38.2 and 44.4°) and Ag₂O (2θ at 38.2) phases, suggesting high dispersion of Ag species in the samples.

Fig. S1 showed N₂ sorption isotherms (A) and pore size distribution (B) of the OMS-2-S, OMS-2-L, 10%Ag/OMS-2-S, and 10%Ag/OMS-2-L catalysts, giving a step at relative pressure (P/P_0) of 0.4 – 0.95 . Correspondingly, their pore size distributions are estimated to be around 20 nm, which are assigned to the pores from aggregation of nanosized crystals of OMS-2 samples. Notably, the specific surface area over the OMS-2 ($81 \text{ m}^2/\text{g}$) is higher than that over the OMS-2-L ($67 \text{ m}^2/\text{g}$). After loading Ag, both the BET surface area and volume were reduced, because the loaded Ag species (Ag⁺, 0.24 nm) can enter the micropores of OMS-2 molecular sieve, which can block the micropores. As a result, the surface area of the Ag loaded OMS-2 catalyst is slightly reduced, as presented in **Table S1**. **Fig. S2** showed SEM images of OMS-2-S and OMS-2-L. They have almost the same needle-like morphology, but the OMS-2-S crystals (~ 20 nm width and 20 – 60 nm long) are much shorter than the OMS-2-L crystals (~ 30 nm width and 100 – 200 nm long).

Figs. 2 and 3 showed HRTEM images and EDS spectra of the 10%Ag/OMS-2-S, and 10%Ag/OMS-2-L. Similarly, it was observed that the crystals of OMS-2-S much shorter than those of OMS-2-L, in good agreement with those in the SEM images.

(Fig. S1). Particularly, it was undetectable for Ag nanoparticles in these HRTEM images, but the signals due to Ag element are very clear in the EDS spectra of 10%Ag/OMS-2-S and 10%Ag/OMS-2-L. These results support that the Ag species are highly dispersed in the Ag/OMS-2 catalysts.

Fig. 4 showed H₂-TPR profiles of the OMS-2-S, OMS-2-L, 10%Ag/OMS-2-S, and 10%Ag/OMS-2-L catalysts. For the OMS-2-S sample, two reduction peaks centered at 259°C and 280°C could be observed, where lower-temperature peak is assigned to the reduction Mn⁴⁺ to Mn³⁺, while higher-temperature peak is related to the reduction Mn³⁺ to Mn²⁺. In the profile of OMS-2-L, only a one peak was observed at around 308°C , which should be mainly attributed to the two steps of MnO₂ reduced to Mn₂O₃ and then to Mn₃O₄ [38]. Notably, after loading Ag species, all reduction peaks are shifted to lower temperature (OMS-2-S: 259°C and 280°C ; Ag/OMS-2-S: 109°C and 141°C ; OMS-2-L: 308°C ; Ag/OMS-2-L: 148°C). These results suggest that the Mn species of OMS-2 are significantly reduced with addition of Ag species, which might be related the presence of hydrogen spillover in the Ag-Mn system [39]. The reducibility of the samples is as follows: OMS-2-L < OMS-2-S < Ag/OMS-2-L < Ag/OMS-2-S. In the meantime, the H₂ consumption was slightly increased (OMS-2-S: 7334 umol/g; Ag/OMS-2-S: 7650 umol/g; OMS-2-L: 7656 umol/g; Ag/OMS-2-L: 8250 umol/g). These

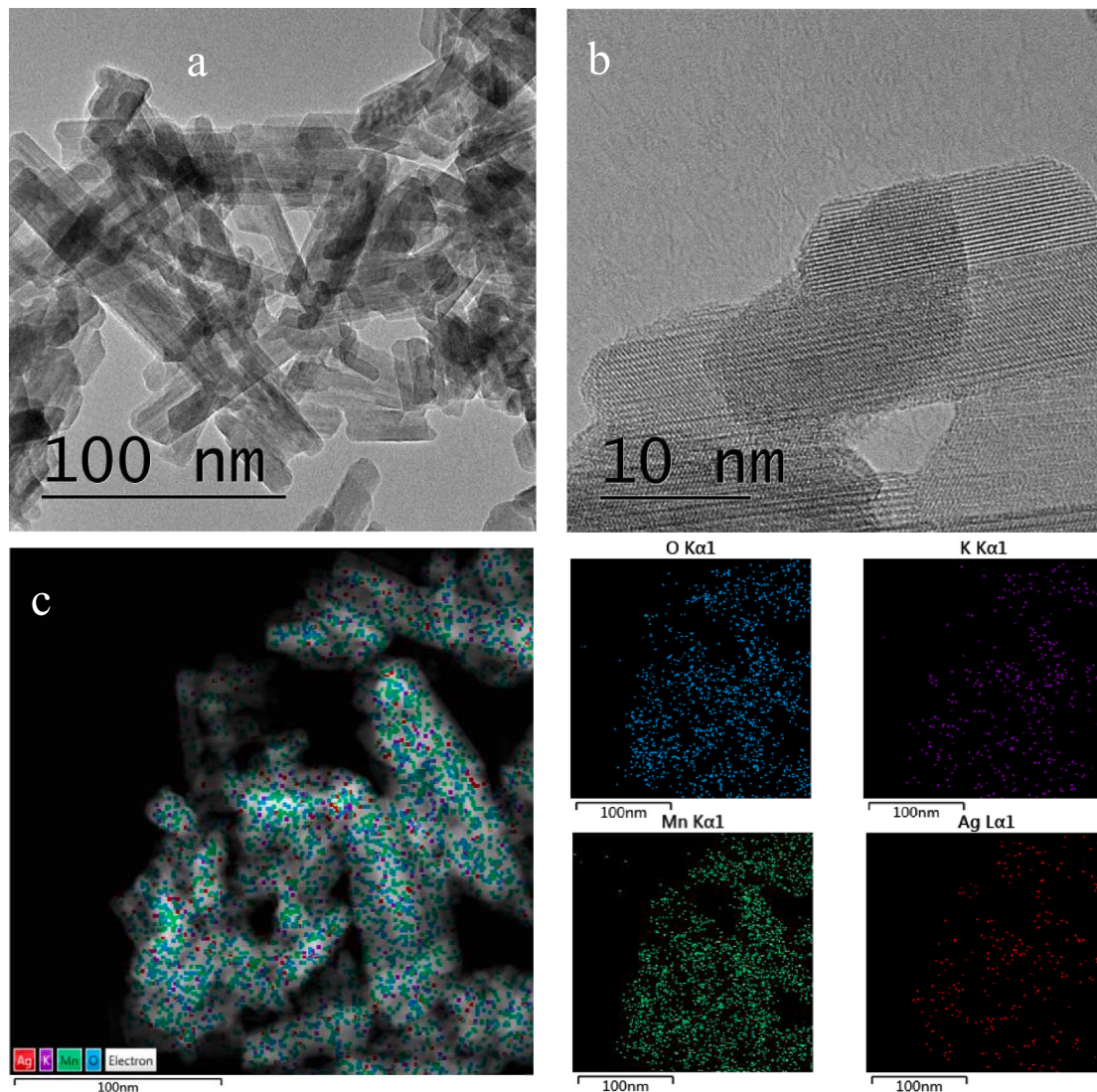


Fig. 2. HRTEM images (a and b) and EDS spectrum (c) of 10%Ag/OMS-2-S.

results indicate that Ag species significantly promote the reduction of OMS-2 [32], which might be related to the spillover of hydrogen from silver atoms to manganese oxides [26,40].

Fig. S3 showed O₂-TPD profiles of the OMS-2-S, OMS-2-L, 10%Ag/OMS-2-S, and 10%Ag/OMS-2-L catalysts, giving two peaks at 500–700 °C and 700–800 °C. The former is the adsorbed oxygen species (O₂, O₂²⁻ or O[·]) close to the surface (active for complete oxidation of HCHO), and the latter is related to the bulk lattice oxygen (O²⁻). Interestingly, after loading Ag species, the adsorbed oxygen species increased significantly, in particular to the 10%Ag/OMS-2-S. These results indicate that 10%Ag/OMS-2-S has more activated oxygen species than the others, which is favorable for oxidation of HCHO at room temperature.

To investigate the adsorption/desorption properties of HCHO in the OMS-2-S, OMS-2-L, 10%Ag/OMS-2-S, and 10%Ag/OMS-2-L samples, HCHO-TPD curves of these catalysts was carried out. As shown in Fig. S4, all samples had similar signal intensity, meaning that these catalysts have similar ability for formaldehyde adsorption.

Fig. S5 and Fig. 5A display Mn2p spectra of the OMS-2-S, OMS-2-L, 10%Ag/OMS-2-S, and 10%Ag/OMS-2-L, giving two peaks at 642.1–642.3 and 654–654.1 eV, which are respectively assigned to Mn 2p_{3/2} and Mn 2p_{1/2}. The peaks at 643.2 and 642 eV could be attributed to the Mn⁴⁺ and Mn³⁺, where the formation of Mn³⁺ species means the presence of oxygen vacancies [41–44], as shown in the following:



where @ represents an oxygen vacancy site. Thus, higher ratio of Mn³⁺/Mn⁴⁺ means higher content of oxygen vacancies in the catalysts. Such oxygen vacancies are beneficial to adsorption and activation of oxygen in the catalysts.

After deconvolution, a quantitative analysis on the Mn 2p_{3/2} spectra was performed and the element molar ratios of Mn³⁺/Mn⁴⁺ are summarized in Table 1. Notably, the Mn³⁺/Mn⁴⁺ ratios in the 10%Ag/OMS-2-S was the highest (1.26), suggesting that the 10%Ag/OMS-2-S has the highest concentration of oxygen vacancies in these catalysts.

Fig. S6 and Fig. 5B showed O1s spectra of the OMS-2-S, OMS-2-L, 10%Ag/OMS-2-S, and 10%Ag/OMS-2-L, giving the binding energies at 529.7–529.9 and 531.5–532 eV, which could be ascribed to lattice oxygen (O²⁻, denoted as O_{latt}) and activated oxygen adsorbed on the sample (denoted as O_{ads}, such as O₂²⁻, O[·] belonging to defect-oxide or hydroxyl-like groups) [14,45,46]. The concentration of O_{ads} species in these catalysts could be estimated, as presented in Table 1. Notably, the 10%Ag/OMS-2-S has the highest concentration of O_{ads} species (29%), which should be helpful for conversion of HCHO molecules [47–49].

Fig. 5 C showed Ag3d spectra of the 10%Ag/OMS-2-S and 10%Ag/OMS-2-L, exhibiting binding energies at 367.6 eV for Ag 3d_{5/2} and 373.6 eV for 3d_{3/2}, which are characteristic of Ag⁺ [50–52], where its

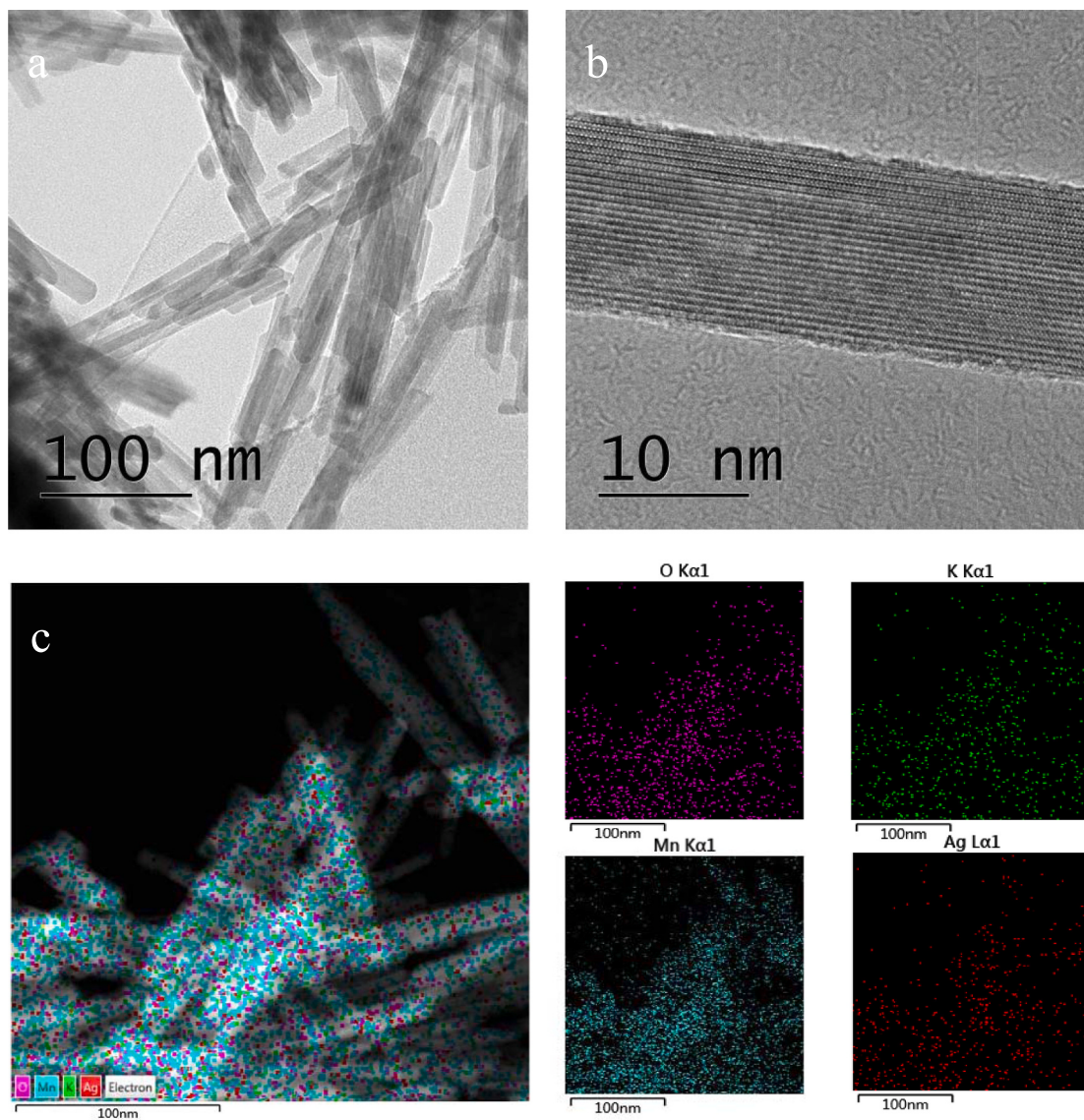


Fig. 3. HRTEM images (a and b) and EDS spectrum (c) of 10%Ag/OMS-2-L.

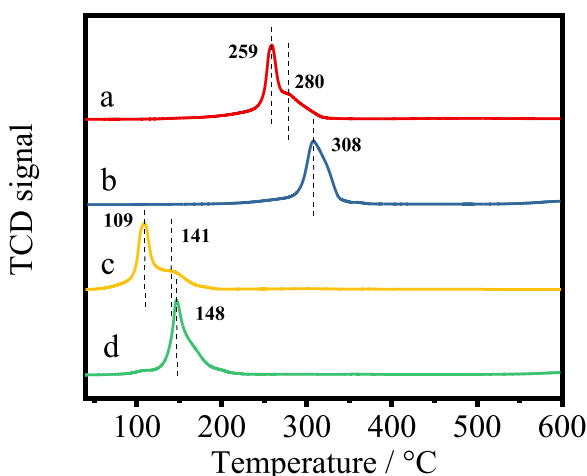


Fig. 4. $\text{H}_2\text{-TPR}$ profiles of the (a) OMS-2-S, (b) OMS-2-L, (c) 10%Ag/OMS-2-S, and (d) 10%Ag/OMS-2-L catalysts.

role is generation of activated oxygen species for oxidation of HCHO. These results confirm that the Ag species are highly dispersed in the catalysts.

3.2. Catalytic evaluation

Fig. 6 showed dependences of catalytic activities on reaction temperature in HCHO oxidation over OMS-2-S, OMS-2-L, 10%Ag/OMS-2-S, and 10%Ag/OMS-2-L catalysts at HCHO concentration of 80 ppm. Before the tests, all catalysts were pretreated in flowing O_2 at 200 °C for 2 h. Notably, OMS-2-S and OMS-2-L catalysts showed complete conversion of HCHO at ca. 85 °C and 90 °C. After loading Ag species, the temperatures for complete conversion of HCHO were significantly reduced, as presented in **Table S2**. For example, the 10%Ag/OMS-2-S showed the complete oxidation of HCHO at low as room temperature (25 °C). This feature is useful for removal of indoor HCHO in daily life. Possibly, the excellent activity of the 10%Ag/OMS-2-S could be contributed to its abundant activated oxygen species in the catalyst, as observed in **Table 1** and **Fig. 5**.

Figs. S7-S8 showed dependences of the catalytic activities on reaction temperature in HCHO oxidation over the Ag/OMS-2 with various Ag loadings, showing that the suitable Ag loading is ca. 10%. The

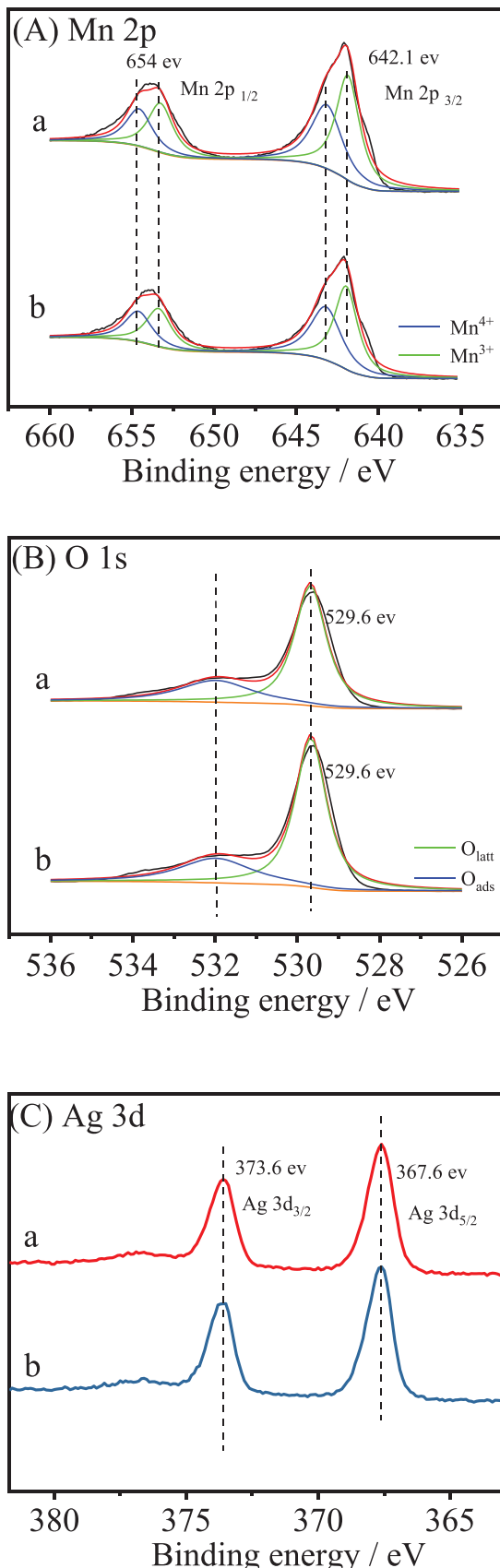


Fig. 5. (A) Mn2p, (B) O1s and (C) Ag3d XPS spectra of (a) 10%Ag/OMS-2-S and (b) 10%Ag/OMS-2-L.

Table 1

Mn2p and O1s XPS spectra of OMS-2-S, OMS-2-L, 10%Ag/OMS-2-S and 10%Ag/OMS-2-L catalysts.

Catalyst	$P(Mn^{3+}/Mn^{4+})^a$	$P(O_{ads})^b$
OMS-2-S	0.74	16.5%
OMS-2-L	0.73	15.1%
Ag/OMS-2-S	1.26	29%
Ag/OMS-2-L	1.18	27.4%

^a Proportion of $Mn^{3+}/Mn^{4+} = \text{Area}(Mn^{3+})/\text{Area}(Mn^{4+})$.

^b Proportion of $O_{ads} = \text{Area}(O_{ads}) / [\text{Area}(O_{ads}) + \text{Area}(O_{latt})] \times 100\%$.

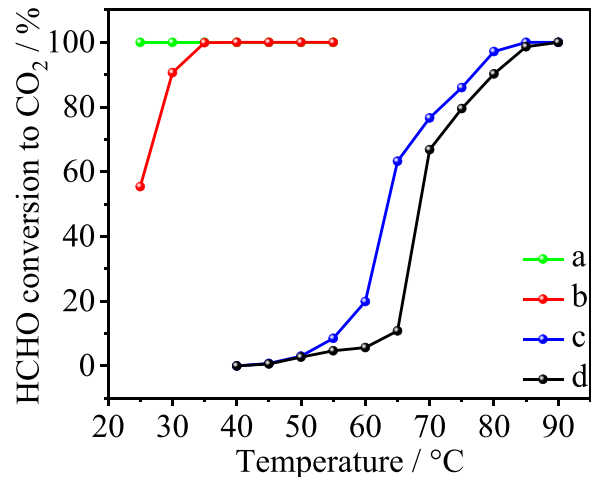


Fig. 6. Dependences of HCHO conversion on reaction temperature in HCHO oxidation over the (a) 10%Ag/OMS-2-S, (b) 10%Ag/OMS-2-L, (c) OMS-2-S, and (d) OMS-2-L catalysts under HCHO concentration of 80 ppm, O₂ 20%, rate of 100 mL/min, space velocity of 60000 mL/g·h, relative humidity of 50%, and He as the balance gas.

temperatures for complete oxidation of HCHO were summarized in Table S3. The results show that the catalytic activities increase with Ag amount when the Ag loadings at 2–8 wt%, and when Ag loadings are over 10 wt%, the catalysts show similar high activities (complete conversion of HCHO at room temperature). Because Ag species are more costly than Mn species, it is suggested that the suitable Ag loading is ca. 10% in the Ag/OMS-2-S catalysts. Fig. S9 showed dependence of complete oxidation temperatures on the HCHO concentration over the 10% Ag/OMS-2-S catalyst, exhibiting that HCHO at 80–200 ppm could be completely oxidized into CO₂ at room temperature. When an initial HCHO concentration was higher than 200 ppm, it required higher temperatures to completely oxidize the formaldehyde. In addition, when the HCHO concentration is reduced to 1 ppm (close to formaldehyde concentration in polluted indoor air), HCHO could be completely oxidized into CO₂ at room temperature (100%, Fig. S10). Fig. S11 showed dependence of HCHO conversion on the reaction temperatures over the 10%Ag/OMS-2-S with various space velocity. It was found that the space velocity had a great effect on activity and higher space velocity needed higher reaction temperature for complete conversion of HCHO. If the relative humidity was changed into higher than 90%, the 10%Ag/OMS-2-S catalyst still remained the complete oxidation of HCHO at room temperature (Fig. S12).

Fig. 7 showed dependences of catalytic activity and selectivity on reaction time under HCHO concentrations of 80 ppm and 3000 ppm, respectively. When the HCHO concentration was 80 ppm, the 10%Ag/OMS-2-S exhibited 100% HCHO conversion and CO₂ selectivity. When the HCHO concentration reached to 3000 ppm, the conversion reduced to 15%, but the selectivity still remained 100% over the 10%Ag/OMS-2-S. These results demonstrate that the 10%Ag/OMS-2-S sample is highly active, very selective, and extraordinarily durable for the complete

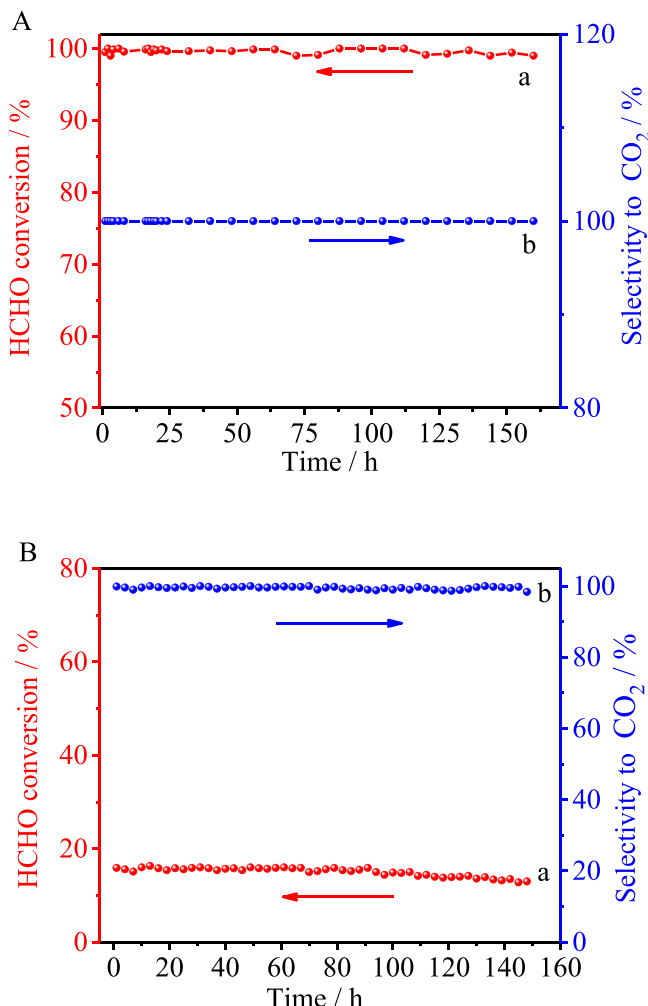


Fig. 7. Dependence of activities on reaction time in HCHO conversion (a) and selectivity to CO₂ (b) over 10%Ag/OMS-2-S catalyst under the conditions of HCHO concentration at (A) 80 ppm and (B) 3000 ppm, O₂ concentration of 20 vol%, He as balance, total flow rate of 100 cm³/min, relative humidity (RH) at 50%, space velocity of 60,000 mL/(g·h), and reaction temperature at 25 °C.

oxidation of HCHO at room temperature.

3.3. Kinetic studies

To understand higher activity in the HCHO oxidation over the Ag/OMS-2-S than that over the other catalysts, the reactant orders of HCHO and oxygen have been investigated according to the equation in the following:

$$\ln R = x \ln [A] + \text{constant}$$

where R is the reaction rate, [A] is the reactant concentration, and x is the reactant order. The x value could be obtained from the slope of a graph of ln R as a function of ln[A], as calculated in Fig. S13 and presented in Table S4. Notably, compared with the other catalysts, the order of oxygen over the Ag/OMS-2-S was significantly reduced, which should be assigned to more O_{ads} species on the Ag/OMS-2-S than those on the other catalysts. In addition, these catalysts displayed almost the same HCHO orders, indicating that there is no any change in the adsorption of HCHO in the catalytic oxidation.

Fig. 8 showed Arrhenius plots for the catalytic oxidation of formaldehyde at the conversion less than 15% over the Ag/OMS-2-S, Ag/OMS-2-L, OMS-2-S, and OMS-2-L catalysts. According to the slopes of Arrhenius plots, we could calculate apparent activation energies (E_a)

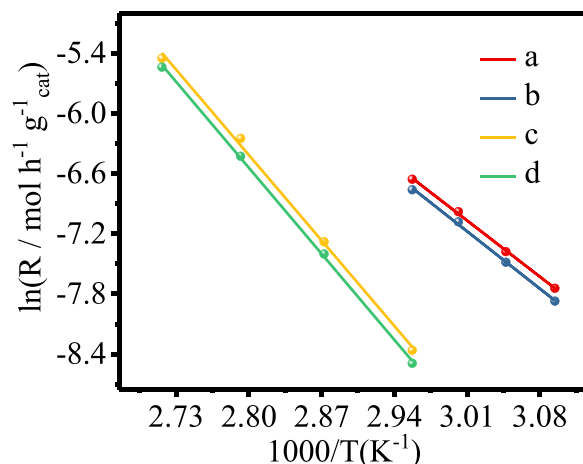
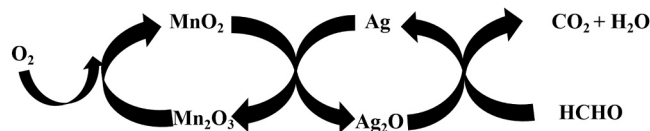


Fig. 8. Arrhenius plots of HCHO oxidation over the (a) Ag/OMS-2-S, (b) Ag/OMS-2-L, (c) OMS-2-S, and (d) OMS-2-L catalysts.

and correlation coefficients (R^2) of the plots lnR versus inverse temperature for the catalytic oxidation of formaldehyde, as summarized in Table S5. The Ag/OMS-2-S and Ag/OMS-2-L catalyst have similar E_a (66 and 67 kJ/mol) values, which are obviously less than those of OMS-2-S and OMS-2-L catalysts (101 and 102 kJ/mol). These results indicate that the addition of Ag species change the active sites.

Normally, the 10%Ag/OMS-2-S catalyst has a strong interaction between silver and manganese species, where an oxygen transfer occurs from Mn⁴⁺/Mn³⁺ to Ag⁺/Ag⁰ [26]. The oxygen species released from Ag⁺/Ag⁰ are very active for oxidation of HCHO into CO₂, as shown in the following:



4. Conclusion

In summary, we have designed an Ag-loaded OMS-2 catalyst from solvent-free route (Ag/OMS-2-S). The Ag/OMS-2-S exhibits high activity, excellent selectivity for CO₂, and extraordinary durability in the complete oxidation of HCHO at room temperature, which are resulted from abundant active oxygen species in the catalyst. The Ag-loaded OMS-2-S catalysts might offer an alternative way for the removal of air pollutants.

CRediT authorship contribution statement

Prof. Feng-Shou Xiao (FSX), Prof. Xiangju Meng (XJM), and Prof. Liang Wang (LW) designed this work, Dr. Ling Zhang (LZ) performed experiments for this work, Dr. Shichao Han (SCH) performed SEM images and ICP experiments, Dr. Yiquan Xie (YQX) and Ms. Yingjuan Wu (YJW) performed TEM images and H₂-TPR experiments. All people discussed the results, and FSX, LZ, and XJM wrote the manuscript.

Declaration of Competing Interest

The authors declare that they have no known competing financial interests or personal relationships that could have appeared to influence the work reported in this paper.

Acknowledgments

This work was supported by National Key Research and Development Program of China (2017YFB0702803), the National Natural Science Foundation of China (U20B6004, 21802123 and 91945302).

Appendix A. Supporting information

Supplementary data associated with this article can be found in the online version at doi:10.1016/j.apcatb.2021.120875.

References

- [1] T. Salthammer, S. Mentese, R. Marutzky, Formaldehyde in the indoor environment, *Chem. Rev.* 110 (2010) 2536–2572.
- [2] B. Bai, Q. Qiao, J. Li, J. Hao, Progress in research on catalysts for catalytic oxidation of formaldehyde, *Chin. J. Catal.* 37 (2016) 102–122.
- [3] S. Rong, T. He, P. Zhang, Self-assembly of MnO₂ nanostructures into high purity three-dimensional framework for high efficiency formaldehyde mineralization, *Appl. Catal. B Environ.* 267 (2020) 118375–118386.
- [4] X. Sun, J. Lin, Y. Wang, L. Li, X. Pan, Y. Su, X. Wang, Catalytically active Ir⁰ species supported on Al₂O₃ for complete oxidation of formaldehyde at ambient temperature, *Appl. Catal. B Environ.* 268 (2020) 118741–118750.
- [5] J. Pei, J. Zhang, On the performance and mechanisms of formaldehyde removal by chemi-sorbents, *Chem. Eng. J.* 167 (2011) 59–66.
- [6] J. Bellat, I. Bezverkhyy, G. Weber, S. Royer, R. Averlant, J. Giraudon, J. Lamonier, Capture of formaldehyde by adsorption on nanoporous materials, *J. Hazard. Mater.* 300 (2015) 711–717.
- [7] G. Qin, Y. Zhang, X. Ke, X. Tong, Z. Sun, M. Liang, S. Xue, Photocatalytic reduction of carbon dioxide to formic acid, formaldehyde, and methanol using dye-sensitized TiO₂ film, *Appl. Catal. B Environ.* 129 (2013) 599–605.
- [8] Q. Huang, Y. Hu, Y. Pei, J. Zhang, M. Fu, In situ synthesis of TiO₂@NH₂-MIL-125 composites for use in combined adsorption and photocatalytic degradation of formaldehyde, *Appl. Catal. B Environ.* 259 (2019) 118106–118119.
- [9] X. Zhu, X. Gao, R. Qin, Y. Zeng, R. Qu, C. Zheng, X. Tu, Plasma-catalytic removal of formaldehyde over Cu-Ce catalysts in a dielectric barrier discharge reactor, *Appl. Catal. B Environ.* 170–171 (2015) 293–300.
- [10] M. Chang, C. Lee, Destruction of formaldehyde with dielectric barrier discharge plasmas, *Environ. Sci. Technol.* 29 (1995) 181–186.
- [11] C. Wang, Y. Li, C. Zhang, X. Chen, C. Liu, W. Weng, W. Shan, H. He, A simple strategy to improve Pd dispersion and enhance Pd/TiO₂ catalytic activity for formaldehyde oxidation: the roles of surface defects, *Appl. Catal. B Environ.* 282 (2021) 119540–119547.
- [12] X. Chen, H. Wang, M. Chen, X. Qin, H. He, C. Zhang, Co-function mechanism of multiple active sites over Ag/TiO₂ for formaldehyde oxidation, *Appl. Catal. B Environ.* 282 (2021), 119543.
- [13] C. Zhang, H. He, A comparative study of TiO₂ supported noble metal catalysts for the oxidation of formaldehyde at room temperature, *Catal. Today* 126 (2007) 345–350.
- [14] B. Bai, H. Arandiyan, J. Li, Comparison of the performance for oxidation of formaldehyde on nano-Co₃O₄, 2D-Co₃O₄, and 3D-Co₃O₄ catalysts, *Appl. Catal. B Environ.* 142 (2013) 677–683.
- [15] C. Shi, Y. Wang, A. Zhu, B. Chen, C. Au, Mn_xCo_{3-x}O₄ solid solution as high-efficient catalysts for low-temperature oxidation of formaldehyde, *Catal. Commun.* 28 (2012) 18–22.
- [16] B. Chen, C. Shi, M. Crocker, Y. Wang, A. Zhu, Catalytic removal of formaldehyde at room temperature over supported gold catalysts, *Appl. Catal. B Environ.* 132–133 (2013) 245–255.
- [17] C. Zhang, F. Liu, Y. Zhai, H. Ariga, N. Yi, Y. Liu, K. Asakura, M. Flytzani-Stephanopoulos, H. He, Alkali-metal-promoted Pt/TiO₂ opens a more efficient pathway to formaldehyde oxidation at ambient temperatures, *Angew. Chem. Int. Ed.* 51 (2012) 9628–9632.
- [18] S. Park, I. Bae, I. Nam, B. Cho, S. Jung, J. Lee, Oxidation of formaldehyde over Pd/Beta catalyst, *Chem. Eng. J.* 195 (2012) 392–402.
- [19] X. Chen, H. Wang, M. Chen, X. Qin, H. He, C. Zhang, Co-function mechanism of multiple active sites over Ag/TiO₂ for formaldehyde oxidation, *Appl. Catal. B Environ.* 282 (2021), 119543, 119543–11955.
- [20] Y. Li, C. Zhang, J. Ma, M. Chen, H. Deng, H. He, High temperature reduction dramatically promotes Pd/TiO₂ catalyst for ambient formaldehyde oxidation, *Appl. Catal. B Environ.* 217 (2017) 560–569.
- [21] J. Chen, M. Jiang, W. Xu, J. Chen, Z. Hong, H. Jia, Incorporating Mn cation as anchor to atomically disperse Pt on TiO₂ for low-temperature removal of formaldehyde, *Appl. Catal. B Environ.* 259 (2019) 118013–118023.
- [22] Z. Huang, X. Gu, Q. Cao, P. Hu, J. Hao, J. Li, X. Tang, Catalytically active singleatom sites fabricated from silver particles, *Angew. Chem. Int. Ed.* 51 (2012) 4198–4203.
- [23] J. Ye, M. Zhou, Y. Le, B. Cheng, J. Yu, Three-dimensional carbon foam supported MnO₂/Pt for rapid capture and catalytic oxidation of formaldehyde at room temperature, *Appl. Catal. B Environ.* 267 (2020) 118689–118696.
- [24] J. Zhang, Y. Li, Y. Zhang, M. Chen, L. Wang, C. Zhang, H. He, Effect of support on the activity of Ag-based catalysts for formaldehyde oxidation, *Sci. Rep.* 5 (2015) 12950–12960.
- [25] L. Ma, D. Wang, J. Li, B. Bai, L. Fu, Y. Li, Ag/CeO₂ nanospheres: efficient catalysts for formaldehyde oxidation, *Appl. Catal. B Environ.* 148 (2014) 36–43.
- [26] X. Tang, J. Chen, Y. Li, Y. Li, Y. Xu, W. Shen, Complete oxidation of formaldehyde over Ag/MnO_x/CeO₂ catalysts, *Chem. Eng. J.* 118 (2006) 119–125.
- [27] C. Mao, M. Vannice, Formaldehyde oxidation over Ag catalysts, *J. Catal.* 154 (1995) 230–244.
- [28] L. Zhang, Y. Xie, Y. Jiang, Y. Li, C. Wang, S. Hang, H. Luan, X. Meng, F.-S. Xiao, Mn-promoted Ag supported on pure siliceous Beta zeolite (Ag/Beta-Si) for catalytic combustion of formaldehyde, *Appl. Catal. B Environ.* 268 (2020) 118461–118466.
- [29] H. Nur, F. Hayati, H. Hamdan, On the location of different titanium sites in Ti-OMS-2 and their catalytic role in oxidation of styrene, *Catal. Commun.* 8 (2007) 2007–2011.
- [30] S. Adjimi, J. Garcia-Vargas, J. Diaz, L. Retailleau, S. Gil, M. Pera-Titus, Y. Guo, A. Giroir-Fendler, Highly efficient and stable Ru/K-OMS-2 catalyst for NO oxidation, *Appl. Catal. B Environ.* 219 (2017) 459–466.
- [31] M. Dinh, T. Giraudon, A. Vandebroucke, R. Morent, N. Geyter, J. Lamonier, Manganese oxide octahedral molecular sieve K-OMS-2 as catalyst in post plasma-catalysis for trichloroethylene degradation in humid air, *J. Hazard. Mater.* 314 (2016) 88–94.
- [32] L. Wang, C. Zhang, H. He, F. Liu, C. Wang, Effect of doping metals on OMS-2/gamma-Al₂O₃ catalysts for plasma-catalytic removal of o-xylene, *J. Phys. Chem. C* 120 (2016) 6136–6144.
- [33] T. Chen, H. Dou, X. Li, X. Tang, J. Li, J. Hao, Tunnel structure effect of manganese oxides in complete oxidation of formaldehyde, *Microporous Mesoporous Mater.* 122 (2009) 270–274.
- [34] M. Ozacar, A. Poyraz, H. Genuino, C. Kuo, Y. Meng, S. Suib, Influence of silver on the catalytic properties of the cryptomelane and Ag-hollandite types manganese oxides OMS-2 in the low-temperature CO oxidation, *Appl. Catal. A Gen.* 462 (2013) 64–74.
- [35] K. Takeuchi, S. Yau, M. Menard, A. Marschilok, E. Takeuchi, Synthetic control of composition and crystallite size of silver hollandite, Ag_xMn₈O₁₆: impact on electrochemistry, *ACS Appl. Mater. Interfaces* 4 (2012) 5547–5554.
- [36] L. Li, D. King, Synthesis and characterization of silver hollandite and its application in emission control, *Chem. Mater.* 17 (2005) 4335–4343.
- [37] Y. Ding, X. Shen, S. Sithambaram, S. Gomez, R. Kumar, V. Crisostomo, S. Suib, M. Aindow, Synthesis and catalytic activity of cryptomelane-type manganese dioxide nanomaterials produced by a novel solvent-free method, *Chem. Mater.* 17 (2005) 5382–5389.
- [38] J. Zhang, Y. Li, L. Wang, C. Zhang, H. He, Catalytic oxidation of formaldehyde over manganese oxides with different crystal structures, *Catal. Sci. Technol.* 5 (2015) 2305–2313.
- [39] R. Xu, X. Wang, D. Wang, K. Zhou, Y. Li, Surface structure effects in nanocrystal MnO₂ and Ag/MnO₂ catalytic oxidation of CO, *J. Catal.* 237 (2006) 426–430.
- [40] S. Hamoudi, A. Sayari, K. Belkacemi, L. Bonneviot, F. Larachi, Catalytic wet oxidation of phenol over Pt_xAg_{1-x}MnO₂/CeO₂ catalysts, *Catal. Today* 62 (2000) 379–388.
- [41] S. Rong, P. Zhang, J. Wang, F. Liu, Y. Yang, G. Yang, S. Liu, Ultrathin manganese dioxide nanosheets for formaldehyde removal and regeneration performance, *Chem. Eng. J.* 306 (2016) 1172–1179.
- [42] J. Jia, P. Zhang, L. Chen, The effect of morphology of α-MnO₂ on catalytic decomposition of gaseous ozone, *Catal. Sci. Technol.* 6 (2016) 5841–5847.
- [43] R. Fang, H. Huang, J. Ji, M. He, Q. Feng, Y. Zhan, D. Leung, Efficient MnO_x supported on coconut shell activated carbon for catalytic oxidation of indoor formaldehyde at room temperature, *Chem. Eng. J.* 334 (2018) 2050–2057.
- [44] X. Liu, K. Zhou, L. Wang, B. Wang, Y. Li, Oxygen vacancy clusters promoting reducibility and activity of ceria nanorods, *J. Am. Chem. Soc.* 131 (2009) 3140–3141.
- [45] P. Prieto, V. Nistor, K. Nouneh, M. Oyama, M. Abd-Lefdl, R. Diaz, XPS study of silver, nickel and bimetallic silver-nickel nanoparticles prepared by seed-mediated growth, *Appl. Surf. Sci.* 258 (2012) 8807–8813.
- [46] Y. Xia, H. Dai, H. Jiang, L. Zhang, J. Deng, Y. Liu, Three-dimensionally ordered and wormhole-like mesoporous iron oxide catalysts highly active for the oxidation of acetone and methanol, *J. Hazard. Mater.* 186 (2011) 84–91.
- [47] J. Yu, X. Li, Z. Xu, W. Xiao, NaOH-modified ceramic honeycomb with enhanced formaldehyde adsorption and removal performance, *Environ. Sci. Technol.* 47 (2013) 9928–9933.
- [48] Z. Xu, J. Yu, W. Xiao, Microemulsion-assisted preparation of a mesoporous Ferrhydrite/SiO₂ composite for the efficient removal of formaldehyde from air, *Chem. Eur. J.* 19 (2013) 9592–9598.
- [49] P. Zhou, X. Zhu, J. Yu, W. Xiao, Effects of adsorbed F, OH, and Cl ions on formaldehyde adsorption performance and mechanism of anatase TiO₂ nanosheets with exposed {001} facets, *ACS Appl. Mater. Interfaces* 5 (2013) 8165–8172.
- [50] H. Huang, Y. Meng, A. Labonte, A. Dobley, S. Suib, Large-scale synthesis of silver manganese oxide nanofibers and their oxygen reduction properties, *J. Phys. Chem. C* 117 (2013) 25352–25359.
- [51] L. Sun, Q. Cao, B. Hu, J. Li, J. Hao, G. Jing, X. Tang, Synthesis, characterization and catalytic activities of vanadium-cryptomelane manganese oxides in low-temperature NO reduction with NH₃, *Appl. Catal. A Gen.* 393 (2011) 323–330.
- [52] J. Chen, X. Tang, J. Liu, E. Zhan, J. Li, X. Huang, W. Shen, Synthesis and characterization of Ag-hollandite nanofibers and its catalytic application in ethanol oxidation, *Chem. Mater.* 19 (2007) 4292–4299.